PHYSICS

Storage and analysis of light-matter entanglement in a fiber-integrated system

Jelena V. Rakonjac[1]†, Giacomo Corrielli[2]†, Dario Lago-Rivera[1]†, Alessandro Seri[1], Margherita Mazzera[3], Samuele Grandi[1]*, Roberto Osellame[2], Hugues de Riedmatten[1,4]

The deployment of a full-fledged quantum internet poses the challenge of finding adequate building blocks for entanglement distribution between remote quantum nodes. A practical system would combine propagation in optical fibers with quantum memories for light, leveraging on the existing communication network while featuring the scalability required to extend to network sizes. Here, we demonstrate a fiber-integrated quantum memory entangled with a photon at telecommunication wavelength. The storage device is based on a fiber-pigtailed laser-written waveguide in a rare earth–doped solid and allows an all-fiber stable addressing of the memory. The analysis of the entanglement is performed using fiber-based interferometers. Our results feature orders-of-magnitude advances in terms of storage time and efficiency for integrated storage of light-matter entanglement and constitute a substantial step forward toward quantum networks using integrated devices.

INTRODUCTION

An interconnected set of quantum hubs will open the way to the next generation of applications in quantum technology, from secure communication to distributed quantum computing (*1*, *2*). The basic ingredient for the realization of these quantum networks is entanglement between light and matter (*3*), distributed over long distances exploiting quantum repeater architectures (*4*, *5*). However, requirements on fidelity and on communication rate and distance place stringent conditions on the physical implementations, which should allow for a high degree of multiplexing and a clear path to scalability. Integrated systems, with a low spatial footprint and enhanced light-matter interaction, provide a promising route forward and already enhanced performances in atomic systems (*6*), quantum dots (*7*), and color centers (*8*, *9*).

Rare earth–based systems (*10*) are excellent candidates for engineering light-matter interactions. Entanglement has already been stored and generated in these systems (*11*–*16*), where photons are mapped into delocalized excitations of billions of ions. These quantum memories support multimode storage (*17*–*19*), and pairing them with an external entanglement source provides a link to entanglement distribution through the telecommunication networks (*15*, *20*) without the need for direct storage at telecommunication wavelengths, which is nevertheless possible in erbium-doped systems (*21*, *22*). The solid-state nature of rare earth–based memories facilitates integration in photonic devices (*23*–*26*), leading to single-ion detection (*27*, *28*) and storage of entanglement in an integrated fashion (*21*, *29*).

In this direction, another key step is to find an efficient way of coupling light in and out of the integrated device. Possible approaches include directly doping an optical fiber with rare earth ions (*21*), where reaching good storage performances is challenging, or adopting free-space coupling (*24*, *29*), limiting the advantages of an integrated device. Alternatively, an integrated structure could be fabricated with a mode that is directly compatible with an optical fiber, which is then attached to the device.

Here, we present a fiber-integrated solid-state system for telecom-compatible light-matter entanglement storage. Our solution is based on a laser-written waveguide in a Y_2SiO_5 crystal doped with praseodymium (Pr) ions (*25*), which is directly coupled and permanently attached (pigtailed) to a single-mode optical fiber. The mode of the waveguide is compatible with that of the fiber, providing an efficient and practical coupling with the integrated device and the stored optical mode, strongly reducing the need for alignment of our optical setup and opening the way to exploiting the resources available to fiber-based and chip-based devices.

RESULTS

A picture of the fiber-pigtailed crystal is shown in Fig. 1A. A type I waveguide is written in the Pr^{3+}:Y_2SiO_5 crystal using femtosecond laser micromachining (*25*). Two single-mode optical fibers are then glued to the facets of the crystal to couple light in and out of the waveguide, with a total transmission of 25% (see Materials and Methods). Our experimental setup is sketched in Fig. 1B. Energy-time entangled pairs of telecom (idler) and visible (signal) photons are generated in a cavity-enhanced spontaneous parametric down-conversion (SPDC) source (*25*), designed to emit narrow photons (1.8 MHz) compatible with light storage in Pr. Signal photons are coupled into a single-mode fiber and directly routed to the fiber-coupled waveguide. The photons are then stored as a collective excitation of the Pr ions for a predetermined storage time using the atomic frequency comb (AFC) protocol (*30*) obtained by shaping the inhomogeneously broadened profile of the $^3H_4(0) \leftrightarrow {}^1D_2(0)$ transition of the Pr ions into a periodic structure (Fig. 1C). The frequency period Δ of the comb determines the storage time of the AFC, as $\tau_{AFC} = 1/\Delta$, such that a photon absorbed by the AFC will be reemitted in the same mode after a time τ_{AFC}. The AFC preparation laser is also guided to the waveguide via the optical fiber, and it is mixed with the signal photons with a 90:10 fiber beam splitter. The fiber-coupled crystal is placed inside a closed-cycle cryostat and cooled to below 3 K. The fiber-to-fiber transmission is maintained

[1]ICFO-Institut de Ciencies Fotoniques, The Barcelona Institute of Science and Technology, Castelldefels (Barcelona) 08860, Spain. [2]Istituto di Fotonica e Nanotecnologie (IFN) - CNR P.zza Leonardo da Vinci 32, Milano 20133, Italy. [3]Institute of Photonics and Quantum Sciences, SUPA, Heriot-Watt University, Edinburgh EH14 4AS, UK. [4]ICREA-Institució Catalana de Recerca i Estudis Avançats, Barcelona 08015, Spain.
*Corresponding author. Email: samuele.grandi@icfo.eu
†These authors contributed equally to this work.

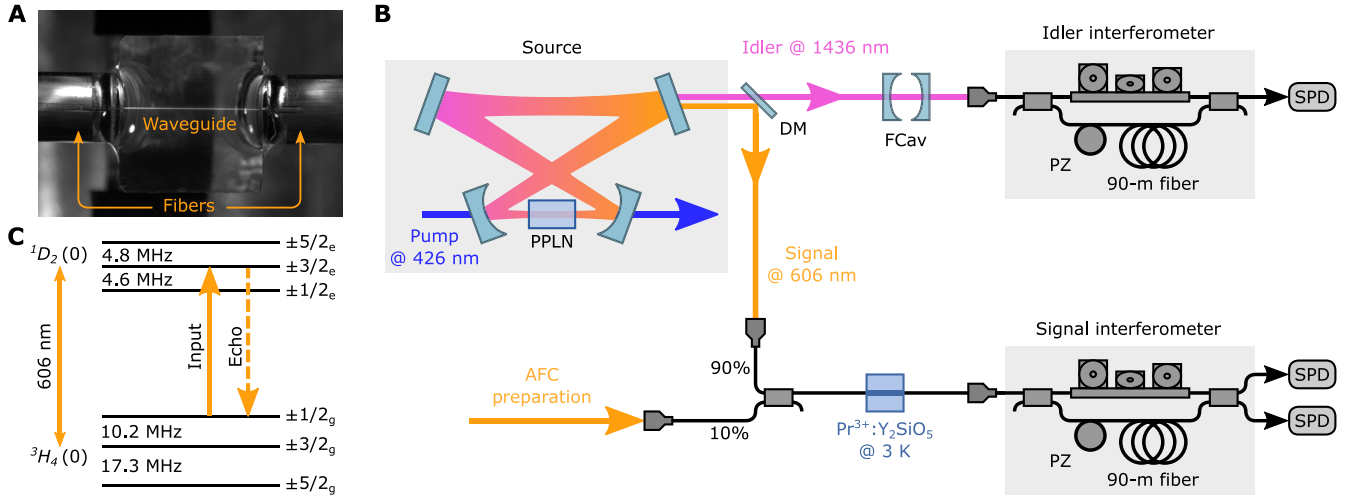

Fig. 1. Experimental setup. (**A**) Picture of the fiber-pigtailed waveguide. The bright line is the fluorescence from the Pr ions, excited by 607-nm light coupled into the waveguide. (**B**) Schematics of the setup. Entangled photon pairs are generated in a cavity-enhanced spontaneous parametric down-conversion (SPDC) source. The idler and the signal are separated by a dichroic mirror (DM), and the latter is coupled to the single-mode fiber that is directly glued to the waveguide in the Pr^{3+}:Y_2SiO_5 crystal, placed inside a cryostat. An AFC of varying storage time is prepared in the memory. The entangled state is analyzed using two fiber-based unbalanced Mach-Zehnder interferometers, with the one for the signal photons directly linked to the waveguide. SPD: single photon detector. The signal photons are detected using silicon photodiodes, while superconducting detectors are used for idler photons. (**C**) Level scheme of Pr^{3+}:Y_2SiO_5.

at low temperatures and through several cooling cycles without substantial deterioration (see Materials and Methods).

We started by measuring the efficiency of the AFC at different storage times and up to 28 μs (see Fig. 2A). The efficiency is defined as the probability that a single photon arriving at the memory is absorbed and then re-emitted in the same mode. It was calculated by comparing the coincidence counts of the AFC echo to those measured, sending the signal photons through a transparency window in the memory (corrected for transmission losses) and with noise counts subtracted. By fitting the data to the function $e^{-4\tau_{AFC}/T_2^{eff}}$ (*31*), we calculate the effective coherence time T_2^{eff} of the AFC storage to be 27(3) μs, an improvement of a factor of 4 with respect to our previous work in the same waveguide without fiber coupling (*25*), which prevented the use of more complex vibration isolation systems. The maximum measured internal efficiency was 18%, corresponding to an end-to-end efficiency of 3.6% (see Materials and Methods). We also measured the second-order cross-correlation function $g^{(2)}_{AFC,i}$ between idler and retrieved AFC echo. The results are reported in Fig. 2B and show that even for our longest storage time, we maintained nonclassical correlations, i.e., $g^{(2)}_{AFC,i} > 2$. Furthermore, we measured the heralded autocorrelation function of the signal photons (*32*) shown in Fig. 3. We measured values of 0.10(3) and 0.05(2) for the case of signal photons going through a transparency window and after storage for 3 μs, respectively. The improvement after the storage is due to the filtering effect of the quantum memory, which shifts the echo away from the SPDC noise.

We then carried out a full tomography of the entangled state of telecom idler and stored signal photon. We used the Franson scheme (*33*) for the analysis, which involves the use of two unbalanced Mach-Zehnder interferometers, one each for the idler and signal photons. The detection of a photon after each interferometer postselects the energy-time entangled state to

$$|\Phi^+\rangle = \frac{|e_i e_s\rangle + |l_i l_s\rangle}{\sqrt{2}} \quad (1)$$

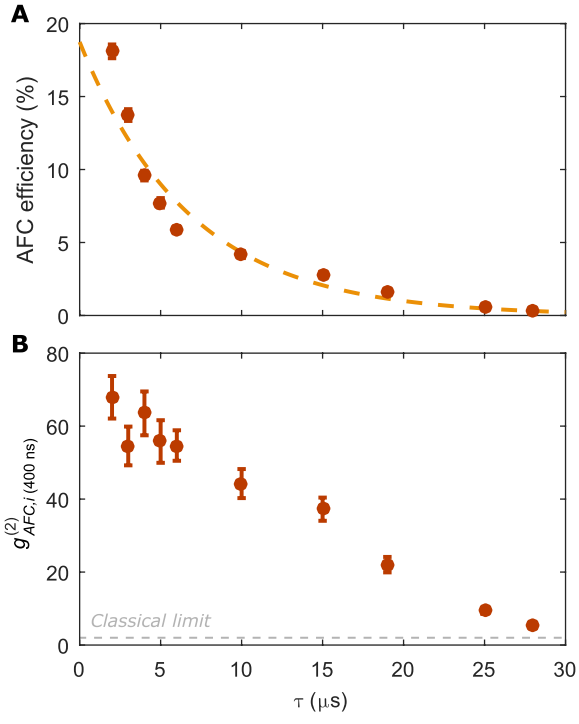

Fig. 2. System characterization at different storage times. (**A**) Efficiency of the AFC for increasing storage time, calculated with single photons in a 400-ns window. The dashed line is a fit to an exponential, from which we were able to extract an effective coherence time T_2^{eff} of 27(3) μs. (**B**) Second-order cross-correlation function $g^{(2)}_{AFC,i}$ between idler photons and retrieved AFC echo for increasing storage time. We measured nonclassical correlations up to the longest storage time we analyzed, 28 μs. For all the plots, the error bars correspond to 1 standard deviation.

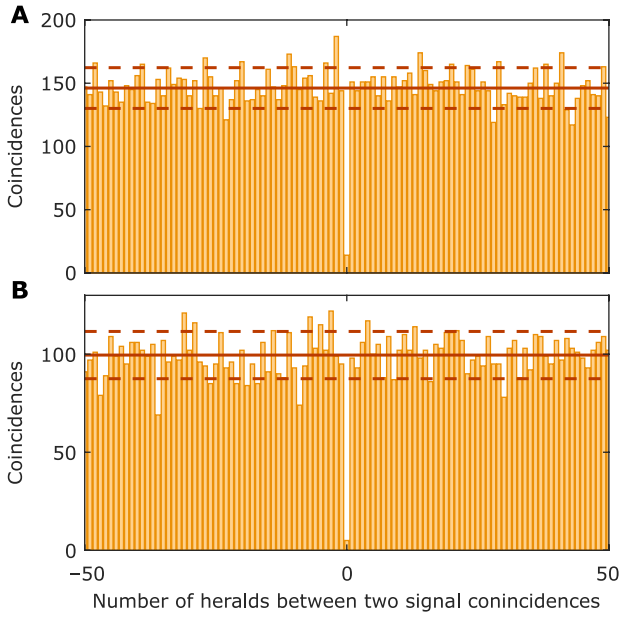

Fig. 3. Heralded autocorrelation. The heralded autocorrelation of signal photons (**A**) going through a transparency window in the quantum memory, or (**B**) stored in a 3-μs AFC. The improvement after AFC storage is a consequence of the filtering effect of the quantum memory, which shifts the interference region away from the SPDC noise. The solid line represents the average of the histograms at long delays, while the dashed lines indicate 1 standard deviation variation from the average.

where $|e\rangle$ (early) and $|l\rangle$ (late) are the two time bins associated with the short and long arm of the interferometer. The state $|\Phi^+\rangle$ then corresponds to a case where the signal and idler photons are in the same time bin, either $|e\rangle$ or $|l\rangle$, with equal probability. Our interferometers are fiber-based (*20*), with the long arm introducing a delay of 420 ns. The relative phase between the two arms can be controlled using piezoelectric fiber stretchers, which changes the base in which the idler and signal modes are measured.

The results of the tomography are reported in Fig. 4. We started by characterizing the heralded qubit and the entangled state generated by the source by preparing a transparency window in the Pr^{3+}:Y_2SiO_5 crystal. We measured an average 1-qubit fidelity for the heralded signal qubit of $\mathcal{F}_{\text{in}}^{1Q} = 87.8(7)\%$, and a 2-qubit fidelity to the ideal state of Eq. 1 of $\mathcal{F}_{\text{in}}^{2Q} = 75(2)\%$ [see the Supplementary Materials for further details, which also references (*34*)]. These values are obtained from raw data and are affected by technical limitations in our analyzers, especially the interferometer for the signal mode as there is a ratio of 50% between the transmission of the long and short arm that limits the visibility to 95%. If we correct for these imperfections and for the dark counts of the detectors, the fidelities become $\widetilde{\mathcal{F}}_{\text{in}}^{1Q} = 91.1(7)\%$ and $\widetilde{\mathcal{F}}_{\text{in}}^{2Q} = 81(2)\%$. These values are still limited by the broadband noise generated by the SPDC and by the limited coherence of the SPDC pump laser.

We then prepared an AFC in the quantum memory with 3 μs of storage time and an efficiency of 13.7(4)%. We repeated the tomography and measured raw fidelities of $\mathcal{F}_{3\mu s}^{1Q} = 89.7(6)\%$ and $\mathcal{F}_{3\mu s}^{2Q} = 79(2)\%$. If corrected, we obtain the values $\widetilde{\mathcal{F}}_{3\mu s}^{1Q} = 93.8(7)\%$ and $\widetilde{\mathcal{F}}_{3\mu s}^{2Q} = 86(2)\%$. These are still limited by the $g_{AFC,i}^{(2)}$ of the retrieved echo after the analyzer and by the quality of the entangled state preparation. However, the fidelities are improved because of the aforementioned temporal filtering of the AFC. Last, we extended the storage time of the AFC to 10 μs, with an efficiency of 4.2(2)%, and repeated the tomography. We obtained fidelities of $\mathcal{F}_{10\mu s}^{1Q} = 88(2)\%$ and $\mathcal{F}_{10\mu s}^{2Q} = 77(3)\%$ for the raw data, and of $\widetilde{\mathcal{F}}_{10\mu s}^{1Q} = 94(2)\%$ and $\widetilde{\mathcal{F}}_{10\mu s}^{2Q} = 86(4)\%$ for the corrected case.

The AFC temporal filtering complicates the comparison of the entangled state before and after the storage, as the input-output fidelity would be lowered despite an improved fidelity with the ideal state after storage. Subtracting the SPDC background from the input state provides a better comparison for the temporally filtered stored AFC state. In this case, the input-output 2-qubit fidelity $\widetilde{\mathcal{F}}_{i/o}^{2Q}$ is 98% and 97% for the 3- and 10-μs storage times, respectively, confirming the reliability of the AFC process and of our device.

DISCUSSION

In this work, we have demonstrated a fiber-integrated quantum memory based on laser-written waveguides. Our results confirm that the entanglement generated by an SPDC process was maintained after a predetermined storage of up to 10 μs in the fiber-coupled integrated memory. We demonstrated an increase in storage time of three orders of magnitude with respect to previous realizations of fiber-integrated quantum memories and an improvement of at least 20 times in terms of efficiency (*21*, *29*), with comparable values of fidelities.

Several improvements are still required to reach a functional device for quantum communication. A natural step forward would be to perform on-demand readout of the stored excitation through storage in a spin ground state of Pr (*17*, *20*, *35*). This has only been demonstrated in a few integrated systems: in a type I (*36*) and type II waveguide (*23*) in Pr^{3+}:Y_2SiO_5 and in a type IV waveguide in $^{151}Eu^{3+}$:Y_2SiO_5 (*37*); however, these works were limited to the storage of classical light. The noise generated by the strong control pulses required for spin-wave storage poses a particular challenge to integrated devices since the stored single photons and the bright controlpulses are in the same spatial mode. On the other hand, the integrated nature of the memory could facilitate the inclusion of narrow laser-written filters, directional couplers, or electrodes for noise-free on-demand storage (*26*, *37*). The limited storage efficiency of the device could be tackled in a similar manner, with improvements in the fiber-to-fiber transmission and with more sophisticated vibration isolation. The intrinsic limitation of the AFC protocol could then be addressed with the inclusion of an impedance-matched cavity (*38*, *39*).

In conclusion, our approach merges the well-explored world of laser-written components, the excellent properties of rare earth–based memories, and the reliability of a fiber-integrated device that is moreover compatible with the telecommunication network. In this framework, entanglement will be stored locally in fiber-coupled quantum memories, while telecom-compatible idler photons are transmitted through the telecom network to perform entanglement swapping operations (*4*, *15*). This combination could allow for an extreme level of multiplexing: Given their size, hundreds of waveguides could be written in a single crystal, exploiting the three-dimensional nature of the fabrication process. This would further maximize the exploitability of temporal and frequency modes (*19*, *40*). An integrated and fiber-coupled quantum memory could be directly interfaced with several fiber-based components, such as fiber arrays, or superconducting detectors, which could be included in the same cryostat without the need for free-space optical access. Moreover,

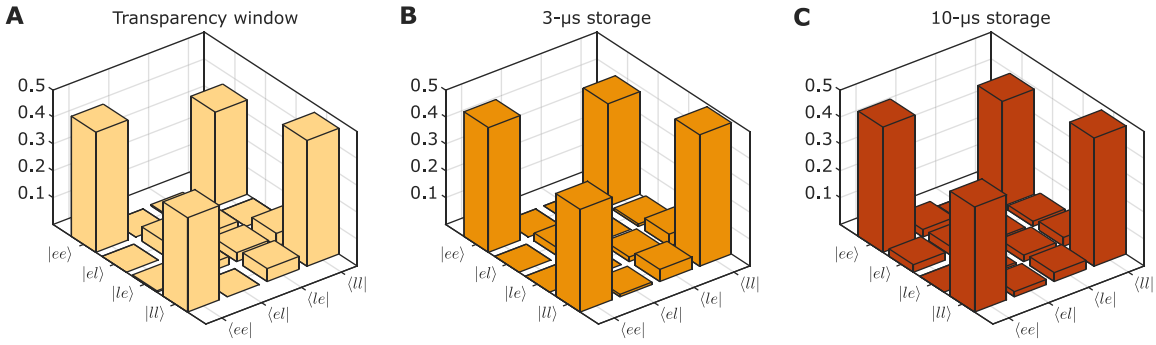

Fig. 4. Entangled state tomography. (**A**) Reconstructed density matrix of the input state, where the signal photon passes through a transparency window in the memory crystal. The data were acquired during 30 min. (**B** and **C**) Density matrices for the retrieved AFC echo for storage times of 3 and 10 μs, respectively. Data acquisition was completed in 120 and 130 min, respectively. Only the real part of the matrices is reported.

type I waveguides feature lower bending losses with respect to other types (*23*, *25*, *26*), which make our device compatible with more involved optical circuitry, allowing for signal routing and filtering. Last, spin-wave storage in Pr opens the way to ultralong storage times (*41*–*43*). Our system will then encompass the basic requirements for a quantum repeater building block, leveraging on its multimodality, fiber compatibility, and scalability.

MATERIALS AND METHODS

Waveguide fabrication and fiber pigtailing

The integrated storage device is based on a type I waveguide femtosecond laser–written in a Pr^{3+}:Y_2SiO_5 crystal (*25*). It was fabricated by focusing the second harmonic of an Yb-based femtosecond laser source (pulse duration of 300 fs, pulse energy of 40 nJ, repetition rate of 20 kHz, and 520-nm wavelength) within the bulk of a Pr^{3+}:Y_2SiO_5 sample with a dopant concentration of 0.05% (grown by Scientific Materials) and by translating the sample along the *b* crystallographic axis at a constant speed of 100 μm/s. The focusing optics used was a 0.65-numerical aperture microscope objective, and the focusing depth was 100 μm below the top surface. The waveguide fabricated in this way supports the propagation of a single mode at 606 nm polarized along the D2 direction, showing a Gaussian mode intensity profile with e^{-2} full widths of 3.1 μm by 6.0 μm. The fiber pigtailing was performed by butt-coupling two 7-m-long fiber patch cables (model 630HP) at both the input and the output of the waveguide and gluing them to the waveguide chip by means of an ultraviolet-curing transparent resin (DELO Photobond GB345). Before gluing, each fiber was cleaved and inserted in a 3-mm-long glass ferrule with external diameter of 1 mm. The e^{-2} diameter of the fiber mode intensity profile, measured at 606 nm, is 2.9 μm. The butt-coupling efficiency is estimated to be 67% per facet by performing the superposition integral between the mode profiles of the fiber and the waveguide, leading to a theoretical maximum transmission efficiency of the overall device of 45%. Waveguide propagation loss, imperfect waveguide facets, and fiber splicing required for mounting the device into the cryostat further reduced the overall transmission to 25%. In perspective, we believe that the best strategy to improve the device transmission consists in optimizing the waveguide irradiation recipe to obtain a more circular profile of the waveguide mode, better matching that of the fiber. Preliminary results in this direction are very promising as we could demonstrate in the laboratory a fiber-to-fiber device transmission as high as 70%.

Entanglement source

To generate narrow photon pairs, we insert a type I periodically poled lithium niobate crystal (PPLN, fabricated by HC Photonics) into an optical cavity. As a consequence, only the photon pairs compatible with the cavity modes will be created. In our case, we pump the PPLN crystal with continuous-wave laser light at 426 nm to produce a signal photon at 606 nm and an idler photon at 1436 nm. Thanks to the cavity, we obtain a biphoton linewidth of 1.8 MHz, compatible with single-class AFC storage in Pr^{3+}ions.

The pump laser is a frequency-doubled laser diode (TOPTICA TA-SHG 110) that generates 426-nm light from a seed at 852 nm through second harmonic generation. A portion of the seed laser is used for Pound-Drever-Hall (PDH) locking to a Fabry-Perot cavity, which ensures that the coherence time of the laser is much greater than the coherence time of the biphotons, allowing for the generation of energy-time entangled photons pairs. The source cavity is locked with the PDH technique using a reference beam taken from the memory preparation. In this manner, the signal photons are at the same frequency as the AFC.

The spectrum of the emission is actually multimode in frequency (*19*). The idler photons are spectrally filtered with a Fabry-Perot cavity (80 MHz of linewidth and 17 GHz of free spectral range), while the signal photons are sent through an etalon filter (4.25 GHz of linewidth and 100 GHz of free spectral range). Moreover, the Pr^{3+}:Y_2SiO_5 crystal, with a transparency window or an AFC, acts as a 4-MHz wide band-pass filter. Idler photons are detected with a superconducting nanowire single photon detector (ID281, from ID Quantique, detection efficiency of 80% and 14 Hz of dark counts), while the signal photons are detected with avalanche single photon counters (COUNT-10C-FC and COUNT-20C-FC, from Laser Components; heralded autocorrelation measurements used COUNT-50C-FC). Detection signals are then analyzed using a time-to-digital converter (Signadyne).

We also studied the correlations between the idler and the signal photons through second-order cross-correlation measurements where $g^{(2)}_{s,i} = \frac{p_{s,i}}{p_s \cdot p_i}$. Here, $p_{s(i)}$ corresponds to the probability of detecting a signal (idler) photon in a time window Δt, while $p_{s,\,i}$ is the probability of detecting a coincidence in that window. We characterized the photon pairs by studying the dependence of $g^{(2)}_{s,i}$ with the

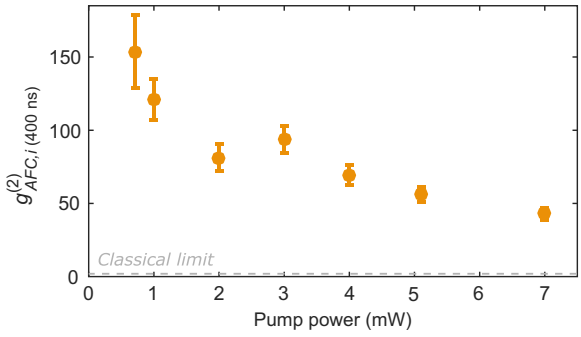

Fig. 5. Correlations with varying pump power. $g^{(2)}_{s,i}$ as a function of the pump power of the SPDC source.

pump power sent to the SPDC source. The results are shown in Fig. 5. For this measurement, we stored the signal photons for 2 μs in the AFC.

Memory setup

The fiber-pigtailed waveguide is placed inside a closed-cycle cryostat (Optistat AC-V14, Oxford Instruments), which cools the sample to about 2.7 K. We designed a special mount for the cryostat to hold the crystal and suppress the strong mechanical vibrations on the cold finger of the cryostat, which comes from the cryostat cycle. The mount sits on springs that decouple the crystal from the vibrations, degrading the coherence of the ions, and has a portion of the optical fiber from the fiber pigtails coiled around it to ensure good thermalization of the sample and to make sure that the crystal and the pigtails move in unison, therefore avoiding further mechanical stress. This vibration isolation system was only possible because our device is fiber-coupled, as, when coupling to it in free space, the transmission through the waveguide would vary because of residual oscillations of the sample induced by the cryostat motion. As mentioned in the Results section, the sample maintained the same transmission through several cooling-and-warming cycles. The fiber-to-fiber transmission through the device, from after the source to after the second fiber-pigtail, dropped from 25 to 20% because of the losses of the splicing points and transmission through the 90:10 beam splitter.

We use a frequency-doubled laser diode (TOPTICA TA-SHG Pro) to generate the light at 606 nm for the preparation of the AFC. The seed laser at 1212 nm is locked through the PDH technique to a home-built Fabry-Perot cavity that reduces its linewidth to <10 kHz. A portion of the laser is used to address Pr ions in the crystallographic site 1 and is shaped in frequency and time using double-pass acousto-optic modulators controlled by a fast arbitrary waveform generator (Signadyne/Keysight). The final preparation light is coupled to the waveguide through a 90:10 fiber beam splitter that is spliced directly to the pigtail of the waveguide. Signal photons are coupled to the memory using the high transmittivity port of the same beam splitter.

Analyzers

We used unbalanced Mach-Zehnder interferometers to perform full qubit tomography in the time domain. Each consists of two arms made out of optical fiber: one short arm with polarization control and one long arm with a 90-m fiber spool and a piezoelectric cylinder with fiber coiled around it. This is used to stretch the optical fiber and stabilize the length difference of the two interferometer arms. The delay introduced by the long arm with respect to the short one is about 420 ns. Besides these common features, the design of the idler interferometer and the signal interferometer differs in the following manner:

Idler interferometer: It is built with SMF28 optical fiber. To stabilize it, we send classical light at 1436 nm, which we obtain through a difference frequency generation (DFG) process inside the SPDC source. This DFG light follows the same optical path as the idler photons, and it is eventually blocked with a chopper wheel to protect the single photon detectors.

Signal interferometer: It is built with 630HP optical fiber. Laser light at 606 nm is injected into the interferometer through its second output and is used as a reference signal for its stabilization. Similar to the previous case, we use synchronized chopper wheels to protect the single photon detectors.

For both interferometers, we use the interference of their respective classical references to obtain a locking signal. We select one point in the interference fringe with a side-fringe lock and the fiber stretcher to maintain the same value of relative phase between the two interferometer arms. We noted that by choosing a locking point in the bottom half of the interference fringe, the system was less sensitive to laser power fluctuations.

SUPPLEMENTARY MATERIALS

Supplementary material for this article is available at https://science.org/doi/10.1126/sciadv.abn3919

REFERENCES AND NOTES

1. H. J. Kimble, The quantum internet. *Nature* **453**, 1023–1030 (2008).
2. S. Wehner, D. Elkouss, R. Hanson, Quantum internet: A vision for the road ahead. *Science* **362**, eaam9288 (2018).
3. L.-M. Duan, M. D. Lukin, J. I. Cirac, P. Zoller, Long-distance quantum communication with atomic ensembles and linear optics. Quantum repeaters with photon pair sources and multimode memories. *Nature* **414**, 413–418 (2001).
4. C. Simon, H. de Riedmatten, M. Afzelius, N. Sangouard, H. Zbinden, N. Gisin, Quantum repeaters with photon pair sources and multimode memories. *Phys. Rev. Lett.* **98**, 190503 (2007).
5. N. Sangouard, C. Simon, H. de Riedmatten, N. Gisin, Quantum repeaters based on atomic ensembles and linear optics. *Rev. Mod. Phys.* **83**, 33–80 (2011).
6. N. V. Corzo, N. V. Corzo, J. Raskop, A. Chandra, A. S. Sheremet, B. Gouraud, J. Laurat, Waveguide-coupled single collective excitation of atomic arrays. *Nature* **566**, 359–362 (2019).
7. R. Uppu, F. T. Pedersen, W. Ying, C. T. Olesen, C. Papon, X. Zhou, L. Midolo, S. Scholz, R.-U. Bochum, A. D. Wieck, A. Ludwig, P. Lodahl, Scalable integrated single-photon source. *Sci. Adv.* **6**, eabc8268 (2020).
8. A. Sipahigil, R. E. Evans, D. D. Sukachev, M. J. Burek, J. Borregaard, M. K. Bhaskar, C. T. Nguyen, J. L. Pacheco, H. A. Atikian, C. Meuwly, R. M. Camacho, F. Jelezko, E. Bielejec, H. Park, M. Lončar, M. D. Lukin, An integrated diamond nanophotonics platform for quantum-optical networks. *Science* **354**, 847–850 (2016).
9. M. K. Bhaskar, R. Riedinger, B. Machielse, D. S. Levonian, C. T. Nguyen, E. N. Knall, H. Park, D. Englund, M. Lončar, D. D. Sukachev, M. D. Lukin, Experimental demonstration of memory-enhanced quantum communication. *Nature* **580**, 60–64 (2020).
10. R. M. Macfarlane, High-resolution laser spectroscopy of rare-earth doped insulators: A personal perspective. *JOL* **100**, 1–20 (2002).
11. C. Clausen, I. Usmani, F. Bussières, N. Sangouard, M. Afzelius, H. de Riedmatten, N. Gisin, Quantum storage of photonic entanglement in a crystal. *Nature* **469**, 508–511 (2011).
12. I. Usmani, C. Clausen, F. Bussières, N. Sangouard, M. Afzelius, N. Gisin, Heralded quantum entanglement between two crystals. *Nat. Photonics* **6**, 234–237 (2012).
13. K. Kutluer, E. Distante, B. Casabone, S. Duranti, M. Mazzera, Time entanglement between a photon and a spin wave in a multimode solid-state quantum memory. H. de Riedmatten, *Phys. Rev. Lett.* **123**, 030501 (2019).
14. M. G. Puigibert, M. F. Askarani, J. H. Davidson, V. B. Verma, M. D. Shaw, S. W. Nam, T. Lutz, G. C. Amaral, D. Oblak, W. Tittel, Entanglement and nonlocality between disparate solid-state quantum memories mediated by photons. *Phys. Rev. Res.* **2**, 13039 (2020).
15. D. Lago-Rivera, S. Grandi, J. V. Rakonjac, A. Seri, H. de Riedmatten, D. Lago-Rivera, S. Grandi, J. V. Rakonjac, A. Seri, H. de Riedmatten, Telecom-heralded entanglement between multimode solid-state quantum memories. *Nature* **594**, 37–40 (2021).
16. X. Liu, J. Hu, Z.-F. Li, X. Li, P.-Y. Li, P.-J. Liang, Z.-Q. Zhou, C.-F. Li, G.-C. Guo, Heralded entanglement distribution between two absorptive quantum memories. *Nature* **594**, 41–45 (2021).

17. A. Seri, A. Lenhard, D. Rieländer, M. Gündoğan, P. M. Ledingham, M. Mazzera, H. de Riedmatten, Quantum correlations between single telecom photons and a multimode on-demand solid-state quantum memory. *Phys. Rev. X* **7**, 021028 (2017).
18. T.-S. Yang, Z.-Q. Zhou, Y.-L. Hua, X. Liu, Z.-F. Li, P.-Y. Li, Y. Ma, C. Liu, P.-J. Liang, X. Li, Y.-X. Xiao, J. Hu, C.-F. Li, G.-C. Guo, Multiplexed storage and real-time manipulation based on a multiple degree-of-freedom quantum memory. *Nat. Commun.* **9**, 3407 (2018).
19. A. Seri, D. L.-Rivera, A. Lenhard, G. Corrielli, R. Osellame, M. Mazzera, H. de Riedmatten, Quantum storage of frequency-multiplexed heralded single photons. *Phys. Rev. Lett.* **123**, 080502 (2019).
20. J. V. Rakonjac, D. Lago-Rivera, A. Seri, M. Mazzera, S. Grandi, H. de Riedmatten, Entanglement between a telecom photon and an on-demand multimode solid-state quantum memory. *Phys. Rev. Lett.* **127**, 210502 (2021).
21. E. Saglamyurek, J. Jin, V. B. Verma, M. D. Shaw, F. Marsili, S. W. Nam, D. Oblak, W. Tittel, Quantum storage of entangled telecom-wavelength photons in an erbium-doped optical fibre. *Nat. Photonics* **9**, 83–87 (2015).
22. I. Craiciu, M. Lei, J. Rochman, J. G. Bartholomew, A. Faraon, Multifunctional on-chip storage at telecommunication wavelength for quantum networks. *Optica* **8**, 114–121 (2021).
23. G. Corrielli, A. Seri, M. Mazzera, R. Osellame, H. de Riedmatten, Integrated optical memory based on laser-written waveguides. *Phys. Rev. Appl.* **5**, 054013 (2016).
24. T. Zhong, J. M. Kindem, J. G. Bartholomew, J. Rochman, I. Craiciu, E. Miyazono, M. Bettinelli, E. Cavalli, V. Verma, S. W. Nam, F. Marsili, M. D. Shaw, A. D. Beyer, A. Faraon, Nanophotonic rare-earth quantum memory with optically controlled retrieval. *Science* **357**, 1392–1395 (2017).
25. A. Seri, G. Corrielli, D. Lago-Rivera, A. Lenhard, H. de Riedmatten, R. Osellame, M. Mazzera, Laser-written integrated platform for quantum storage of heralded single photons. *Optica* **5**, 934–941 (2018).
26. C. Liu, T.-X. Zhu, M.-X. Su, Y.-Z. Ma, Z.-Q. Zhou, C.-F. Li, G.-C. Guo, On-demand quantum storage of photonic qubits in an on-chip waveguide. *Phys. Rev. Lett.* **125**, 260504 (2020).
27. A. M. Dibos, M. Raha, C. M. Phenicie, J. D. Thompson, Atomic source of single photons in the telecom band. *Phys. Rev. Lett.* **120**, 243601 (2018).
28. J. M. Kindem, A. Ruskuc, J. G. Bartholomew, J. Rochman, Y. Q. Huan, A. Faraon, Control and single-shot readout of an ion embedded in a nanophotonic cavity. *Nature* **580**, 201–204 (2020).
29. E. Saglamyurek, N. Sinclair, J. Jin, J. A. Slater, D. Oblak, F. Bussières, M. George, R. Ricken, W. Sohler, W. Tittel, Broadband waveguide quantum memory for entangled photons. *Nature* **469**, 512–515 (2011).
30. M. Afzelius, C. Simon, H. de Riedmatten, N. Gisin, Multimode quantum memory based on atomic frequency combs. *Phys. Rev. A* **79**, 052329 (2009).
31. P. Jobez, N. Timoney, C. Laplane, J. Etesse, A. Ferrier, P. Goldner, N. Gisin, M. Afzelius, Towards highly multimode optical quantum memory for quantum repeaters. *Phys. Rev. A* **93**, 032327 (2016).
32. S. Fasel, O. Alibart, S. Tanzilli, P. Baldi, A. Beveratos, N. Gisin, H. Zbinden, High-quality asynchronous heralded single-photon source at telecom wavelength. *J. Phys.* **6**, 163 (2004).
33. J. D. Franson, Bell inequality for position and time. *Phys. Rev. Lett.* **62**, 2205–2208 (1989).
34. J. B. Altepeter, D. F. James, P. G. Kwiat, 4 Qubit quantum state tomography, in *Quantum State Estimation*, M. Paris, J. Řeháček, Eds. (Springer, 2004), pp. 113–145.
35. M. Gündoğan, P. M. Ledingham, K. Kutluer, M. Mazzera, H. de Riedmatten, Solid state spin-wave quantum memory for time-bin Qubits. *Phys. Rev. Lett.* **114**, 230501 (2015).
36. A. Seri, "A multimode solid-state quantum memory for single photons," thesis, Universitat Politècnica de Catalunya (2019).
37. C. Liu, Z. Q. Zhou, T. X. Zhu, L. Zheng, M. Jin, X. Liu, P. Y. Li, J. Y. Huang, Y. Ma, T. Tu, T. S. Yang, C. F. Li, G. C. Guo, Reliable coherent optical memory based on a laser-written waveguide. *Optica* **7**, 192–197 (2020).
38. M. Afzelius, C. Simon, Impedance-matched cavity quantum memory. *Phys. Rev. A* **82**, 022310 (2010).
39. J. H. Davidson, P. Lefebvre, J. Zhang, D. Oblak, W. Tittel, Improved light-matter interaction for storage of quantum states of light in a thulium-doped crystal cavity. *Phys. Rev. A* **101**, 042333 (2020).
40. N. Sinclair, E. Saglamyurek, H. Mallahzadeh, J. A. Slater, M. George, R. Ricken, M. P. Hedges, D. Oblak, C. Simon, W. Sohler, W. Tittel, Spectral multiplexing for scalable quantum photonics using an atomic frequency comb quantum memory and feed-forward control. *Phys. Rev. Lett.* **113**, 053603 (2014).
41. C. Laplane, P. Jobez, J. Etesse, N. Gisin, M. Afzelius, Multimode and long-lived quantum correlations between photons and spins in a crystal. *Phys. Rev. Lett.* **118**, 210501 (2017).
42. Y. Ma, Y.-Z. Ma, Z.-Q. Zhou, C.-F. Li, G.-C. Guo, One-hour coherent optical storage in an atomic frequency comb memory. *Nat. Commun.* **12**, 2381 (2021).
43. A. Ortu, A. Holzäpfel, J. Etesse, M. Afzelius, Storage of photonic time-bin qubits for up to 20 ms in a rare-earth doped crystal. *NJP Quantum Inf.* **8**, 29 (2022).

Acknowledgments

Funding: This project received funding from the European Research Council (ERC) via the advanced grant CAPABLE (742745), from the European Union Horizon 2020 research and innovation program within the Flagship on Quantum Technologies through grant 820445 (QIA), under grant agreement no. 899275 (DAALI) of the FET-Open funding call, and under the Marie Skłodowska-Curie grant agreement no. 713729 (ICFOStepstone 2) and no. 754510 (proBIST), from Laserlab Europe (grant agreement no. 654148), from the Gordon and BettyMoore Foundation through grant GBMF7446 to H.d.R., and from the government of Spain (PID2019-106850RB-I00, Severo Ochoa CEX2019-000910-S, BES-2017-082464), Fundació Cellex, Fundació Mir-Puig, and Generalitat de Catalunya (CERCA, AGAUR, Quantum CAT).

Author contributions: G.C. fabricated the waveguide and realized the fiber-pigtailing. G.C., M.M., J.V.R., A.S., and S.G. contributed to the mounting and adapting of the sample to the cryostat. J.V.R. and D.L.-R. acquired and analyzed data, with J.V.R. operating the quantum memory setup and D.L.-R. operating the entanglement source. D.L. and S.G. designed and assembled the fiber interferometers. S.G. analyzed the tomography data and wrote the paper, with input from all coauthors. R.O. and H.d.R. supervised the project. **Competing interests:** The authors declare that they have no competing interests. **Data and materials availability:** All data needed to evaluate the conclusions in the paper are present in the paper and/or the Supplementary Materials.

Submitted 3 December 2021
Accepted 23 May 2022
Published 8 July 2022
10.1126/sciadv.abn3919